Environmental Science
Nano

ROYAL SOCIETY
OF CHEMISTRY

PAPER
Joel A. Pedersen *et al.*
Formation of supported lipid bilayers containing phase-segregated
domains and their interaction with gold nanoparticles

175 YEARS

PAPER

CrossMark
click for updates

Formation of supported lipid bilayers containing phase-segregated domains and their interaction with gold nanoparticles†

Eric S. Melby,[ad] Arielle C. Mensch,[b] Samuel E. Lohse,‡[c] Dehong Hu,[d] Galya Orr,[d] Catherine J. Murphy,[c] Robert J. Hamers[b] and Joel A. Pedersen*[ab]

For nanoparticles that have been released into the environment, the cell membrane represents an initial site of interaction with eukaryotic cells. The encounter of nanoparticles with cellular membranes may alter membrane structure and function, lead to uptake into cells, or elicit adverse biological responses. Supported lipid bilayers have proven to be valuable *ex vivo* models for biological membranes, allowing investigation of their mechanisms of interaction with nanoparticles with a degree of control impossible in living cells. To date, the majority of research on nanoparticle interaction with supported lipid bilayers has employed membranes composed of single or binary mixtures of phospholipids. Cellular membranes contain a wide variety of lipids and exhibit lateral organization. Ordered membrane domains enriched in specific membrane components, also referred to as lipid rafts, have not been explored with respect to their interaction with nanoparticles. Here we develop model membranes containing segregated domains differing in fluidity that are amenable to investigation by a variety of surface-sensitive analytical techniques and demonstrate that these domains influence the extent of nanoparticle attachment to model membranes. We determined conditions that allow reliable formation of bilayers containing liquid-ordered domains enriched in sphingomyelin and cholesterol and confirmed their morphology by structured illumination and atomic force microscopies. We demonstrate that the presence of liquid-ordered domains increases attachment of cationic gold nanoparticles to model membranes relative to those lacking such domains under near physiological ionic strength conditions (0.1 M NaCl) at pH 7.4. We anticipate that these results will serve as the foundation for and motivate further study of nanoparticle interaction with phase-segregated domains.

Nano impact

The interaction of nanoparticles with cellular membranes can be a critical determinant in eliciting adverse outcomes in organisms. Model membranes composed of single or binary phospholipid mixtures have provided insight into the interaction with nanomaterials. Cytoplasmic membranes of living organisms, however, are made up of hundreds of components laterally organized into dynamic functional domains. We have established a platform to investigate the interaction of nanoparticles with model membranes containing ordered lipid domains with a variety of surface-sensitive analytical techniques. We demonstrate that the presence of these domains influences the interaction of cationic gold nanoparticles with model membranes under high ionic strength conditions. This study highlights the need to systematically investigate the interaction of nanoparticles with important membrane components and structures.

[a] *University of Wisconsin-Madison, Environmental Chemistry and Technology Program, 1525 Observatory Dr., Madison, WI 53706, USA. E-mail: joelpedersen@wisc.edu*
[b] *University of Wisconsin-Madison, Department of Chemistry, 1101 University Ave., Madison, WI 53706, USA*
[c] *University of Illinois at Urbana-Champaign, Department of Chemistry, 600 S. Mathews Ave., Urbana, IL 61801, USA*
[d] *Environmental Molecular Sciences Laboratory, Pacific Northwest National Laboratory, Richland, WA 99352, USA*
† Electronic supplementary information (ESI) available. See DOI: 10.1039/c5en00098j
‡ Present address: Colorado Mesa University, Department of Chemistry, 1100 North Ave, Grand Junction, CO, 81501.

Introduction

The cytoplasmic membrane serves as an initial point of contact between eukaryotic cells and nanomaterials that have been either intentionally or inadvertently released into the environment.[1] Nanoparticle interactions at these nano-bio interfaces[2] include attachment,[3] passive penetration, endocytotic uptake,[4] membrane permeabilization,[5,6] and toxicological insult due to nanoparticle dissolution, generation of reactive oxygen species, or oxidative stress.[7] If nanoparticles are

This journal is © The Royal Society of Chemistry 2016

Environ. Sci.: Nano, 2016, **3**, 45–55 | 45

internalized, they can also interact with the membranes that bound organelles including lysosomes, mitochondria, and the nucleus.[8]

Mechanistic understanding of nanomaterial interaction with the cellular membranes of eukaryotes requires consideration of chemical composition, physical properties, and lateral organization of these critical structures. Cellular membranes are composed of a complex mixture of phospholipids, sphingolipids, sterols, and peripheral, integral and lipid-anchored proteins. Sphingolipids, phosphatidylinositol (a class of phospholipids) and membrane proteins can bear glycans, which can vary in composition and size. Cellular membranes typically contain several hundred lipid species when differences in headgroup, acyl chain length, the number and location of unsaturated bonds, and degree of glycosylation are taken into account.[9,10] The lipid distribution between the inner and outer leaflet of biological membranes is typically asymmetric.[11] The majority lipid components in the outer leaflet of animal cytoplasmic membranes are zwitterionic phosphatidylcholine and sphingomyelin, and neutral cholesterol.[12] Minority lipid components in the outer leaflet of these membranes include zwitterionic phosphatidylethanolamine and the anionic phospholipids phosphatidylserine, (phosphorylated) phosphatidylinositol, and phosphatidic acid.[13] Lipid molecules in cellular membranes not only provide a barrier function, but also participate in signaling processes and membrane trafficking.[14]

Cellular membranes are laterally organized, exhibiting domains differing in composition and lipid order. Domains of higher lipid order and enriched in specific membrane components are sometimes referred to as lipid rafts. These highly ordered domains are enriched in sphingolipids and cholesterol, and the acyl chains of majority of raft lipids are saturated.[12] The degree of acyl chain saturation and preferential lipid association with sterols result in lipid segregation into a distinct liquid-ordered (L_o) phase, the components of which are, to a large degree, segregated from those of the liquid-disordered (L_d) phase.[15] For the purposes of this paper we refer to segregated L_o domains in supported lipid bilayers as "domains". The L_o phase is a highly ordered and tightly packed phase similar to the gel phase, but with much higher lateral mobility.[12] The existence of lipid rafts in eukaryotic cellular membranes has been debated since the concept was introduced in 1997.[16] The primary source of this debate is the small size and transient nature of lipid rafts within membranes,[17,18] with typical length scales <50 nm and time scales on the order of milliseconds.[19,20] A definition for these structures was developed at the Keystone Symposium on Lipid Rafts and Cell Function in 2006: "Membrane rafts are small (10–200 nm), heterogeneous, highly dynamic sterol- and sphingomyelin-enriched domains that compartmentalize cellular processes".[21] At the time of writing, the lateral organization of biological membranes is a topic of intense research. Further refinement of the lipid raft concept is expected as new techniques are brought to bear on understanding membrane structure.[22] The rafts in cellular

membranes are credited with a variety of functions, including preferential association by some membrane proteins,[16] mediation of sorting in the trans-Golgi network,[23] endocytotic pathway sorting,[24] and signaling in hematopoietic cells.[25] Membrane rafts appear to be ubiquitous features of cellular membranes; evidence exists for their presence in animal,[12] plant,[26] fungal,[27] and bacterial[28] cell membranes.

Supported lipid bilayers have proven to be useful models for biological membranes, allowing mechanisms of their interaction with nanomaterials to be studied with a degree of control impossible in living cells.[29–31] Lipid bilayers on solid supports can be probed with a variety of optical,[31] acoustic[30–33] and scanning probe[34–36] techniques. Among these techniques, quartz crystal microbalance with dissipation monitoring (QCM-D) and atomic force microscopy (AFM) allow label-free and *in situ* investigation of supported lipid bilayers. To date, most studies examining nanoparticle interaction with such model membranes have been restricted to supported lipid bilayers composed of single and binary mixtures of phospholipids.[31,35–39] Despite the importance of lipid rafts in organismal membranes, investigation of nanoparticle interaction with these features of cellular membranes has not been previously reported. Prior studies have demonstrated successful formation of supported lipid bilayers containing phase-segregated domains on mica (by AFM)[40] and optical glass (by fluorescence microscopy).[41] Formation of domain-containing supported lipid bilayers on QCM-D sensors has been attempted,[42] but success has not been demonstrated.

The objectives of this study were to develop a method to form model membranes containing phase-segregated domains on QCM-D sensor surfaces and to investigate the influence of such domains on nanoparticle attachment to model membranes. In this study, we employed a model membrane system comprising three components: the unsaturated phospholipid 1,2-dioleoyl-*sn*-glycero-3-phosphocholine (DOPC), the sphingolipid N-stearoyl-D-*erythro*-sphingosylphosphorylcholine (octadecanoyl sphingomyelin, SM), and the sterol lipid cholesterol (Chol). Sphingomyelin has a high affinity for Chol, which results in dense lipid packing and the formation of L_o regions (domains) within a L_d phase.[43,44] To accomplish the first objective, we varied experimental parameters and the ratios of lipids in the ternary mixture to form supported lipid bilayers on planar SiO_2 substrates by the vesicle fusion method.[32,33] We confirmed the formation of supported lipid bilayers containing phase-segregated domains using a combination of QCM-D, AFM, and super-resolution fluorescence structured illumination microscopy (SIM). To achieve the second objective, we probed nanoparticle interactions with these domains using 4 nm gold nanoparticles (AuNPs) functionalized with anionic or cationic ligands by QCM-D.

Materials and methods

Materials

The following lipids were purchased from Avanti Polar Lipids (Alabaster, AL): 1,2-dioleoyl-*sn*-glycero-3-phosphocholine

(DOPC, 850375C), *N*-stearoyl-D-*erythro*-sphingosylphosphorylcholine (SM, 860586P), plant-derived cholesterol (Chol, 700100P), ganglioside G_{M1} (860065P), and TopFluor PC (810281C). We procured Atto647N DOPE from Atto-Tec (Siegen, Germany). Hydrogen tetrachloroaurate trihydrate ($HAuCl_4 \cdot 3H_2O$), sodium borohydride, and mercaptopropanoic acid were purchased from Sigma-Aldrich. We obtained 3-amino propanethiol hydrochloride from MolPort Chemicals. Solid NaCl and Tris were obtained from Sigma-Aldrich, and all buffer solutions were made in ultrapure water (18.2 MΩ cm; Barnstead Nanopure) and filtered through a Millex GP 220 nm PES filter cartridge. PALL tangential flow filtration capsules (50 kDa pore size) were purchased from VWR. SiO/Cu mesh transmission electron microscopy grids were obtained from TedPella. All materials were used as received, unless otherwise noted.

Formation and characterization of small unilamellar vesicles

Small unilamellar vesicles were prepared by the extrusion method.[32,45] Just prior to use, SM and Chol were dissolved in chloroform (Sigma Aldrich). DOPC, SM, and Chol were mixed to the desired ratio, and the chloroform was evaporated under a stream of ultrapure N_2 gas. For some fluorescent studies, 1 mol% ganglioside G_{M1} dissolved in 60 : 32 : 8 chloroform : ethanol : water (by volume), 0.1 mol% TopFluor PC, and/or 0.1 mol% Atto647N DOPE was included prior to evaporation under a stream of ultrapure N_2 gas. The dried lipid films were held under vacuum for at least 1 h, rehydrated in 0.001 M NaCl, pH 7.4 (10 mM Tris) buffer to a stock concentration of 1.25 mg mL^{-1}, subjected to three freeze (liquid N_2)/ thaw (bath sonicator) cycles to ensure complete sample mixing,[46] and extruded 11 times through 50 nm polycarbonate membranes (Avanti Polar Lipids, 610003) with an extruder set (Avanti Polar Lipids, 610 000). The resulting small unilamellar vesicles were stored at 4 °C and used within one week. A 0.03 mg mL^{-1} solution of the small unilamellar vesicles (diluted in either 0.001 or 0.1 M NaCl, pH 7.4 (0.01 M Tris)) was used to determine their hydrodynamic diameter (d_h) by dynamic light scattering and zeta potential (ζ) by laser Doppler microelectrophoresis (Malvern Zetasizer Nano ZS). The literature is not unified in the definition of small unilamellar vesicles. For the purpose of this study we define small unilamellar vesicles as vesicles with diameters smaller than 100 nm.[32] The size and ζ for small unilamellar vesicles containing SM and Chol (and G_{M1}) and those composed solely of DOPC were similar (Table 1).

Gold nanoparticle synthesis and characterization

Thiol-stabilized 4 nm AuNPs were synthesized using previously reported methods.[47,48] In an *aqua regia*-cleaned 500 mL round bottom flask, 400 mL of ultrapure water, 1.5 mL of $HAuCl_4$ (0.1 M), and either 200 μL of NaOH (1.0 M) and 1.5 mL of 0.1 M mercaptopropionic acid (MPA) or 1.8 mL of HCl (0.1 M) and 3.5 mL of 0.1 M mercaptopropylamine (MPNH$_2$) were combined, and stirred at vortex for 10 min. These

Table 1 Hydrodynamic diameter (d_h) and zeta potential (ζ) values for small unilamellar vesicles used in this study. The DOPC : SM : Chol molar ratios were 60 : 20 : 20. Ganglioside G_{M1} was incorporated at 1 mol%. Solutions were buffered to pH 7.4 with 0.01 M Tris and contained the indicated amount of NaCl

Small unilamellar vesicles	d_h (nm)		ζ (mV)	
	0.001 M NaCl	0.1 M NaCl	0.001 M NaCl	0.1 M NaCl
DOPC	71 ± 3	67 ± 2	−17 ± 1	−1.6 ± 1.0
DOPC/SM/Chol	78 ± 4	80 ± 8	−21 ± 1	−1.6 ± 1.1
DOPC/SM/Chol + G_{M1}	79 ± 3	73 ± 2	−23 ± 1	−3.1 ± 0.7

additions produced a clear, colorless solution. (***Warning: aqua regia is a strong oxidant and highly corrosive.***) After the initial stirring, either 5.0 mL of a 0.1 M aqueous sodium borohydride solution (for MPA–AuNPs) or 35 mL of ice–cold 0.01 M aqueous sodium borohydride solution (for MPNH$_2$– AuNPs) was added to the solution. The solution rapidly turns brown, then red-orange. The resulting red-orange AuNP solution was stirred for 3 h. The crude AuNP solution was then purified by diafiltration.[47] The 500 mL AuNP solution was concentrated to an initial volume of 50 mL and purified by passing 3.0 L of ultrapure water through the diafiltration system.

Gold nanoparticle core size and concentration were determined from their UV-vis spectra.[49] Core size was confirmed by transmission electron microscopy (Fig. S1†). A 10 nM solution of the synthesized AuNPs (diluted in either 0.001 or 0.1 M NaCl, pH 7.4 (0.01 M Tris)) was used to determine AuNP hydrodynamic diameter (d_h) by dynamic light scattering and apparent zeta potential (ζ^{app}) by laser Doppler microelectrophoresis (Malvern Zetasizer Nano ZS). All AuNP concentrations are expressed as number concentrations.

Quartz crystal microbalance with dissipation monitoring

All QCM-D experiments were conducted using the Q-Sense E4 system containing four silica-coated sensors (QSX 303) mounted in temperature-controlled, liquid flow cells (QFM 401; Biolin Scientific, Göteborg, Sweden). Quartz crystal microbalance with dissipation monitoring measures changes in the resonance frequency and energy dissipation induced by the interaction of an analyte with the surface of a coated piezoelectric quartz crystal. Frequency shifts (Δf) reflect changes in mass coupled to the sensor surface (analyte mass + hydrodynamically coupled water). Changes in the energy dissipation (ΔD) are related to the viscoelastic properties of laterally homogeneous adlayers or to the properties of the particle-surface contact region for films of discrete nanoscale objects.[50]

The QCM-D silica sensor crystals were prepared for use by bath sonication in a 2% solution of sodium dodecyl sulfate for 20 min, rinsing consecutively with ethanol and ultrapure water three times, drying with ultrapure N_2 gas, and UV/ozone

This journal is © The Royal Society of Chemistry 2016

Environ. Sci.: Nano, 2016, **3**, 45–55 | 47

treatment for 30 min (Bioforce Nanosciences UV/Ozone Procleaner). Supported lipid bilayers were formed by the vesicle fusion method.[32] Briefly, after mounting the sensors in the flow cells, 0.1 M NaCl, pH 7.4 (0.01 M Tris) buffer was allowed to flow over the sensors until frequency and dissipation values stabilized. A suspension of small unilamellar vesicles (0.03 mg mL^{-1}) was then allowed to flow across the sensor until stable values of Δf and ΔD were obtained after passing through a minimum and maximum, respectively, that indicate attainment of a critical adsorbed vesicle concentration, commencement of vesicle rupture, and supported lipid bilayer formation.[51] The supported lipid bilayer was then rinsed with vesicle-free buffer for 15 min to remove any adhering vesicles. All experiments used a constant flow rate of 0.1 mL min^{-1} and temperature of 25 °C unless otherwise noted. Variables that were tested in arriving at conditions to form L_o domain-containing bilayers included vesicle concentration, solution ionic strength during vesicle deposition, the ionic strength of the rinsing solution, timing of the initiation of the rinsing step, and temperature. Specifically, we examined small unilamellar vesicle introduction in high ionic strength solutions (up to 0.15 M NaCl), temperature elevation to 35 °C after small unilamellar vesicle introduction, rinsing with low ionic strength (0.025 M NaCl) solutions, initiation of rinsing immediately after the rupture event, and vesicle introduction at temperatures up to 35 °C. The key modification allowing successful formation of L_o domain-containing supported lipid bilayers was the decrease in vesicle concentration relative to the previously published attempt to form such bilayers,[42] which eliminated the adsorption of vesicles to the supported lipid bilayer.

After successful formation of supported lipid bilayers, for nanoparticle attachment experiments conducted at 0.1 M NaCl, pH 7.4 (0.01 mM Tris), nanoparticles were diluted to a concentration of 10 nM with the same buffer and flowed over the supported lipid bilayer for 20 min. The supported lipid bilayer was then rinsed with buffer for 20 min to assess the reversibility of nanoparticle attachment. Otherwise, for nanoparticle attachment experiments conducted at 0.001 M NaCl, pH 7.4 (0.01 mM Tris), after bilayer formation and rinsing the buffer was switched to 0.001 M NaCl for at least 10 min to allow a stable baseline to be attained, and the subsequent dilution of nanoparticles to 10 nM and rinsing were conducted in this buffer solution. We assessed the attachment of both MPNH$_2$– and MPA–AuNPs to DOPC-only, 60/20/20 mol% DOPC/SM/Chol, and 60/20/20 mol% DOPC/SM/Chol with 1 mol% G_{M1} supported lipid bilayers. The initial rate of nanoparticle attachment to the supported lipid bilayers was determined as described previously.[52] Briefly, the QCM-D Δf curve was subjected to locally weighted scatterplot smoothing (LOESS; α = 0.1),[53] and the one minute moving Δf rate was averaged for the first 5 min of nanoparticle attachment to the supported lipid bilayer to determine the initial rate of nanoparticle attachment. All attachment experiments were conducted in triplicate. Data comparisons were made by

one-way ANOVA with a Tukey post-hoc test at the $p \leq 0.05$ level of significance.

Structured illumination microscopy

Imaging was carried out using a Zeiss Elyra fluorescence microscope with a 63× objective. Supported lipid bilayers were formed under batch conditions within 35/22 mm #1.5 glass bottom dishes (Willco Wells). Dishes were rinsed with ultrapure water (18.2 MΩ cm; MilliQ Advantage A10, Millipore), dried with N$_2$, and cleaned in a UV/Ozone chamber (PSD Pro Series, Novascan) for 20 min. The 0.1 M NaCl, pH 7.4 (0.01 M Tris) buffer solution was introduced to the clean dishes at least 20 min prior to vesicle introduction. Suspensions of small unilamellar vesicles (0.06 mg mL^{-1} containing either 0.1 mol% TopFluor PC (λ_{ex} = 488 nm; λ_{em} = 503 nm) or 0.1 mol% Atto647N DOPE (λ_{ex} = 642 nm; λ_{em} = 667 nm) and sometimes 1 mol% ganglioside G_{M1} in the same buffered solution) were introduced to the dish, and bilayer formation was monitored by confocal fluorescence microscopy. We were able to distinguish unruptured vesicles from lipid bilayers using fluorescence recovery after photobleaching (FRAP; see below) because unruptured vesicles do not diffuse laterally, and as a result, they do not recover after photobleaching; in contrast, the lipids within supported lipid bilayers are able to diffuse in and out of the monitored region, resulting in recovery upon photobleaching. Upon bilayer formation, the solution contained within the dish was exchanged five times with 2 mL aliquots of the buffered solution. Two separate fluorescent phospholipids were used to ensure our observed results could not be attributed to the inclusion of the fluorophore. Additionally, these two fluorescent phospholipids were chosen because they differ in both the excitation/emission wavelengths of the fluorophore as well as the location of the fluorophore. TopFluor is covalently conjugated to one of the lipid acyl chains, while Atto647N is covalently conjugated to the lipid headgroup.

Fluorescence recovery after photobleaching

To determine supported lipid bilayer formation and phospholipid diffusion coefficients, we conducted FRAP experiments using a Zeiss LSM 710 microscope with a scan rate of 240 ms. A minimum of eight FRAP curves from two different supported lipid bilayers were analyzed to obtain diffusion coefficients. Fluorescence intensities were normalized to that of the initial supported lipid bilayer. Data were analyzed using a nonlinear least-squares fitting method to determine the characteristic diffusion time, τ_D, using the equation:[54,55]

$$F(t) = \frac{F(0) + F(\infty)(t/\beta\tau_D)}{1 + (t/\beta\tau_D)}$$

where $F(t)$ is the observed relative fluorescence as a function of time, $F(0)$ is the relative fluorescence intensity immediately following the bleach pulse, $F(\infty)$ is the relative fluorescence intensity at infinite time following the bleach pulse, β is the bleach depth given by $1 - F(0)$, and τ_D is the characteristic

48 | Environ. Sci.: Nano, 2016, 3, 45–55

This journal is © The Royal Society of Chemistry 2016

diffusion time. The lateral diffusion coefficient, D, was then determined using

$$D = \omega^2/4\tau_D$$

where ω is the bleach spot radius. Image processing was carried out using ImageJ software.

Atomic force microscopy

Images were collected in tapping mode using a Nanoscope IV controller (Digital Instruments) with a Type J scanner. Silicon nitride probes (Bruker, DNP) with a force constant of 0.35 N m^{-1} and a MTFML-V2 probe holder were used to collect images in fluid. Bilayers were formed on ultra-flat B-doped silicon wafers with a 200 nm thermal oxide layer (Ted Pella) under the same conditions as those described for QCM-D. To image under flow conditions (0.1 mL min^{-1}, 25 °C), the wafer was first equilibrated in 0.1 M NaCl, pH 7.4 (0.01 M Tris) buffer for 20 min, vesicle solution (0.03 mg mL^{-1}) was flowed for 20 min, the bilayer was rinsed with buffer for 20 min, and the bilayer was imaged. The L$_o$ domains investigated here are readily observable in AFM as contiguous regions appearing higher than the surrounding regions. Initial image analysis was conducted with Gwyddion.[56] Quantitative analysis of AFM data was performed using Igor Pro (Wavemetrics, Lake Oswego, OR, USA) to import the image data, calculate histograms of the height distributions, and then fit the histogram to two Gaussian distributions. The area of the peak corresponding to the higher height distribution (domains) was divided by the total area to give a fractional coverage of the L$_o$ domains.

Results and discussion

Formation of supported lipid bilayers containing phase-segregated domains

We first established a set of experimental conditions that allowed supported lipid bilayers to be formed on silica-coated QCM-D sensors from vesicles composed of 60/20/20 mol% DOPC/SM/Chol. Based on final stable $\Delta f_5/5$ and ΔD_5 values in QCM-D experiments,[30,32,33] we determined that supported lipid bilayers could be formed from these small unilamellar vesicles at a vesicle concentration of 0.03 mg mL^{-1} in 0.1 M NaCl at pH 7.4 (0.01 M Tris) and 25 °C. Representative frequency and dissipation traces (Fig. 1) for formation of supported lipid bilayers under these conditions from vesicles composed of DOPC or 60/20/20 mol% DOPC/SM/Chol reflect the two-step process commonly observed in the formation of bilayers of zwitterionic lipids on silica substrates: attainment of a critical adsorbed vesicle concentration followed by initiation of vesicle rupture and formation of the supported bilayer.[32,51] The final frequency and dissipation values for the DOPC bilayer were −24.9 ± 0.1 Hz and 0.17 (±0.02) × 10^{-6}, respectively, consistent with prior reports of supported lipid bilayer formation from similar phospholipids.[32] For supported bilayers formed from 60/20/20 mol%
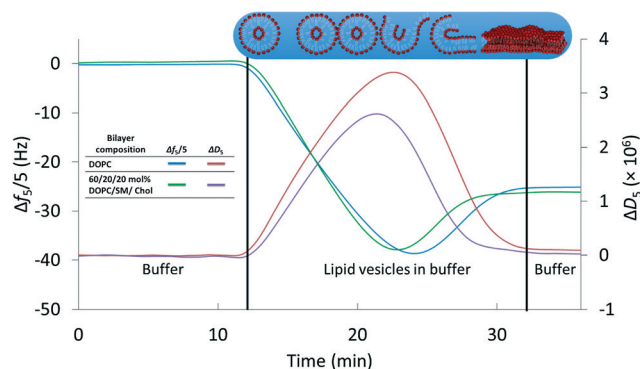

Fig. 1 Formation of supported lipid bilayers from small unilamellar vesicles composed of DOPC or 60/20/20 mol% DOPC/SM/Chol as monitored by QCM-D. Final resonant frequency changes were −24.9 ± 0.1 Hz and −26.8 ± 0.6 Hz for the DOPC and DOPC/SM/Chol bilayers, respectively (n = 3). The corresponding dissipation values were 0.17 (±0.02) × 10^{-6} and 0.51 (±0.29) × 10^{-6}. Overall supported lipid bilayer formation kinetics were similar for the two compositions. Data are shown from the 5th harmonic and were subjected to LOESS smoothing (α = 0.1).[53] The buffer solution was 0.01 M Tris (pH 7.4) in 0.1 M NaCl.

DOPC/SM/Chol the final $\Delta f_5/5$ value was −26.8 ± 0.6 Hz, more negative than that for the pure DOPC bilayer. The more negative frequency value of 60/20/20 mol% DOPC/SM/Chol bilayer corresponds to higher bilayer mass than for the pure DOPC bilayer. We attribute the higher mass of the 60/20/20 mol% DOPC/SM/Chol bilayer to the interaction of sphingomyelin with cholesterol,[57] increasing lipid packing density relative to pure DOPC. The final dissipation value for 60/20/20 mol% DOPC/SM/Chol bilayers was 0.51 (±0.29) × 10^{-6}, higher than that for DOPC bilayers.

We employed super-resolution fluorescence structured illumination microscopy to determine whether the supported lipid bilayers formed from 60/20/20 mol% DOPC/SM/Chol vesicles contained phase-segregated domains with the expected morphology. Structured illumination microscopy allows fluorescence images to be obtained with sub-diffraction limit (~100 nm) resolution.[58,59] Such super-resolution capabilities were critical because domains can have dimensions smaller than the diffraction limit of light, making these structures largely invisible to standard fluorescence microscopy techniques.[60] Supported lipid bilayers were formed from vesicles containing one of two fluorescently labeled phospholipids, both of which were expected to segregate to the L$_d$ regions with DOPC. We therefore expected to observe a fluorescent signal in the L$_d$ regions and the absence of a fluorescent signal in the L$_o$ domains. Fig. 2A and B show SIM images of 60/20/20 mol% DOPC/SM/Chol supported lipid bilayers that contain TopFluor PC and Atto647N DOPE, respectively. Both images display areas of fluorescent signal and patches of dark regions consistent with the presence of L$_o$ domains that exclude the fluorescent phospholipids. To determine whether the dark regions were indeed L$_o$ domains composed of SM and Chol, as opposed to being large defects in the bilayer, we formed supported lipid

This journal is © The Royal Society of Chemistry 2016
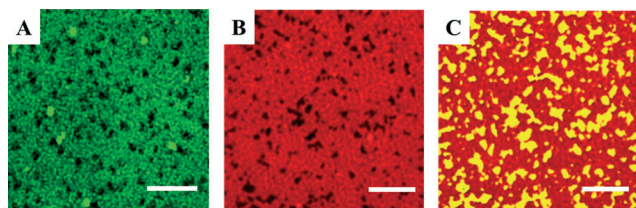
Environ. Sci.: Nano, 2016, **3**, 45–55 | 49

Fig. 2 A–C. Structured illumination microscopy images displaying the exclusion of fluorescently-labeled (A) TopFluor PC (green) and (B) Atto647N DOPE (red) phospholipids from dark regions that are expected to be L_o domains in supported lipid bilayers composed of 60/20/20 mol% DOPC/SM/Chol with 0.1 mol% fluorescent phospho-lipid. To confirm the dark regions are L_o domains, 1 mol% G_{M1} was incorporated into the vesicles prior to formation supported lipid bilay-ers and is expected to segregate to the L_o domains.[40] Alexa555-labeled cholera toxin subunit B protein (yellow) binds G_{M1}, and its pres-ence in the dark regions (C) confirms the dark regions are L_o domains. Scale bars are 2 μm.

Fig. 3 Atomic force microscopy confirms (A) the presence of distinct L_o and L_d phases with (B) the expected ~1 nm height difference between phases in a supported lipid bilayer consisting of 60/20/20 mol% DOPC/SM/Chol. (C) The coverage of L_o domains was determined by fitting the AFM image height distribution. Scale bar is 2 μm. AFM images of other compositions investigated are provided in Fig. S2.†

bilayers from small unilamellar vesicles with the same compo-sition as above, but also containing 1 mol% ganglioside G_{M1}. Ganglioside G_{M1} segregates to L_o domains[40] and is the cell surface receptor for cholera toxin B (CTB) homopentamer, with each CTB pentamer binding five G_{M1} molecules.[61,62] We used the binding of fluorescently labeled CTB (Alexa555-labeled CTB pentamer; Life Technologies) to G_{M1} to confirm that the dark regions were L_o domains. The SIM image in Fig. 2C displays the fluorescence of this cholera toxin B homo-pentamer in the dark regions that exclude the fluorescent phospholipids, confirming the existence of L_o domains.

We further investigated the morphology and extent of L_o domains in these supported lipid bilayers by AFM. The majority of prior AFM studies of phase-segregated domains in planar bilayers has focused on model membranes supported on mica[57] or glass coverslips.[60] We formed L_o domain-containing bilayers on silica substrates to provide a direct connection with our QCM-D experiments. Fig. 3 dis-plays an AFM image of a 60/20/20 mol% DOPC/SM/Chol supported lipid bilayer with a corresponding height profile and height distribution. These data confirm the presence of domains in the supported lipid bilayer that differ in height by ~1 nm. This result is consistent with prior studies that indicate that L_o domains are approximately 1 nm thicker than L_d regions due to the cholesterol-induced ordering of the unsaturated acyl chains of sphingomyelin.[57] We note that the AFM data indicate that the bilayer is free from surface adsorbed vesicles, which would be evident due to their large size (70–80 nm; Table 1) relative to the height of the supported lipid bilayer. Therefore, the higher final dissipa-tion value for bilayers composed of 60/20/20 mol% DOPC/SM/Chol relative to those composed of pure DOPC does not appear attributable to the presence of intact vesicles adhering to the bilayer.

To further characterize these L_o domain-containing supported lipid bilayers, we examined the lateral diffusivity of phospholipids within the L_d phase by FRAP. From these experiments we determined the lateral diffusion coefficient
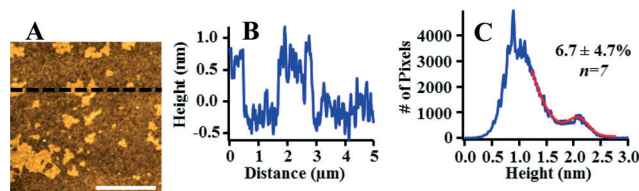
for TopFluor PC, which our SIM experiments confirmed to segregate to the L_d regions, to be 1.81 ± 0.16 μm^2 s^{-1}. This value agrees well with previous reports of fluorescent lipid dif-fusion in L_d regions ranging from 1.47 to 2.12 μm^2 s^{-1}.[46,63–65]

We next explored the compositional space bounded by the limits of sphingomyelin (0–30%) and cholesterol content (10–50%) in typical eukaryotic membranes.[14] The ternary phase diagram in Fig. 4 displays the boundaries for the phases expected for various combinations of the three com-ponents used in our experiments based on prior work with intact giant unilamellar vesicles (10–100 μm).[66] In this figure, we indicate the compositions of vesicles from which we suc-cessfully formed supported lipid bilayers based on the obser-vation of the characteristic two-phase formation kinetics in QCM-D experiments and the final stable $\Delta f_5/5$ and ΔD_5 values (Table 2). The final $\Delta f_5/5$ and ΔD_5 values for bilayers formed from the ternary lipid mixtures were slightly more negative and more positive, respectively, than those formed from pure DOPC. The ternary lipid mixtures from which supported bilayers formed spanned a compositional range that included
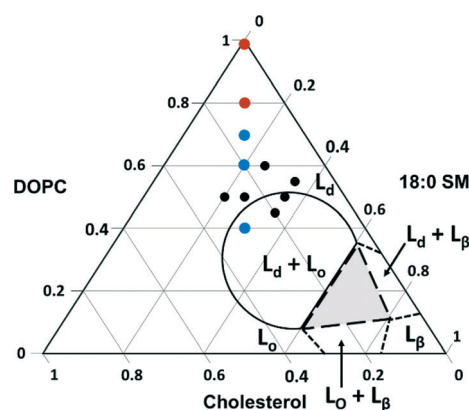

Fig. 4 Ternary phase diagram showing the composition of vesicles from which supported lipid bilayers were successfully formed on SiO_2 substrates as monitored by QCM-D. Black dots represent compositions investigated by QCM-D alone, and colored dots indicate those compositions (imaged by AFM) that resulted in segregated L_o domain formation (blue) and those that resulted in a single continuous phase (red). Lines indicate expected phase boundaries based on studies of giant unilamellar vesicles.[66]

Table 2 Final changes in frequency (Δf) and dissipation factor (ΔD) for supported lipid bilayers formed from vesicles varying in DOPC/SM/Chol composition. Values presented are for the 5th harmonic after the introduction of small unilamellar vesicles and rinsing with vesicle-free buffer for 15 min. All measurements were conducted in triplicate

mol% DOPC/SM/Chol	$\Delta f_5/5_{final}$ (Hz)	ΔD_5 ($\times 10^{-6}$)
100/0/0	−24.9 ± 0.1	0.17 ± 0.02
80/10/10	−25.9 ± 0.4	0.20 ± 0.01
70/15/15	−27.5 ± 1.3	0.46 ± 0.02
60/20/20	−26.8 ± 0.6	0.51 ± 0.29
60/25/15	−27.0 ± 0.5	0.35 ± 0.07
55/35/10	−27.6 ± 0.2	0.24 ± 0.02
50/20/30	−28.3 ± 0.3	0.47 ± 0.20
50/25/25	−27.8 ± 0.6	0.43 ± 0.03
50/35/10	−27.6 ± 0.2	0.24 ± 0.02
45/35/20	−28.0 ± 0.3	0.54 ± 0.16
40/30/30	−29.2 ± 0.6	0.52 ± 0.17

Fig. 5 Supported lipid bilayer formation time (t_{SLB}) as a function of vesicle cholesterol content as monitored by QCM-D. Supported lipid bilayer formation time was calculated from the time that vesicles were first observed adhering to the sensor surface to the time of initiation of vesicle rupture (as evidenced by the abrupt decrease in ΔD_5). Fit ($y = 0.077x + 4.782$) was obtained using a standard least squares analysis ($R^2 = 0.82$).

segregated L_o and L_d phases as well as a single continuous L_d phase in studies with giant unilamellar vesicles.[66]

To determine the vesicle compositions that yielded domain-containing supported lipid bilayers, as well as to verify that intact vesicles were not adsorbed to the bilayer surfaces, we examined selected supported lipid bilayers by AFM (*viz.* those comprised of 40/30/30, 70/15/15, 80/10/10, and 100/0/0 mol% DOPC/SM/Chol; red and blue dots in Fig. 4). Representative images, height profiles, and L_o domain coverages are shown in Fig. S2.† All bilayers containing domains exhibit the expected ~1 nm height difference between L_o and L_d regions, and no intact vesicles were observed across the compositions investigated. These images indicate that within the compositional space examined, L_o domain formation is expected for supported lipid bilayers containing 15 mol% SM and Chol or more. Referring to the phase diagram boundaries (Fig. 4), phase-segregation does not occur in giant unilamellar vesicles at SM and Chol concentrations below ~27 mol%.[66] Our results agree with a previous fluorescence microscopy study on domain formation in supported lipid bilayers that demonstrated phase segregation in bilayers containing ≥15 mol% Chol and sphingomyelin.[67]

To determine the impact of vesicle composition on supported lipid bilayer formation kinetics, we examined supported lipid bilayer formation time (defined as the time from vesicle adsorption to initial rupture) as a function of vesicle Chol content (Fig. 5). This analysis indicates that increasing Chol content in small unilamellar vesicles lengthens the time to initiation of vesicle rupture, consistent with a prior report.[42] The lengthening of time to vesicle rupture is attributed to the ability of Chol to quickly flip-flop between the two bilayer leaflets.[68] Vesicles flatten when adsorbed to silica surfaces,[69] and the ability of Chol to flip-flop between leaflets reduces the stress of vesicle flattening. Often, the attraction of vesicles to a solid surface, and their subsequent flattening, is insufficient to promote supported lipid bilayer formation. Inter-vesicle interaction has an additional destabilizing effect on adsorbed vesicles that promotes vesicle fusion and ultimately supported lipid bilayer
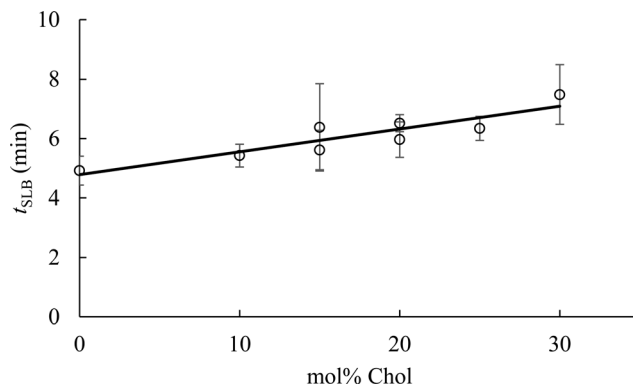
formation.[70] The observation that supported lipid bilayer formation time increased with Chol content suggests that a larger inter-vesicle interaction force is required to overcome the vesicle stabilization caused by Chol flip-flop.

Interaction of anionic and cationic gold nanoparticles with L_o domain-containing supported lipid bilayers

As a first step toward understanding the influence of phase-segregated domains on nanoparticle interaction with model membranes, we compared the attachment of cationic and anionic AuNPs to supported lipid bilayers containing L_o domains (60/20/20 mol% DOPC/SM/Chol ± 1 mol% G_{M1}) with those composed of pure DOPC in QCM-D experiments. The AuNPs had 4 nm spherical cores (Fig. S1†) and were functionalized with cationic mercaptopropyl amine (MPNH$_2$) or anionic mercaptopropionic acid (MPA). Attachment experiments were conducted in 0.001 M and 0.1 M NaCl at pH 7.4 (0.01 M Tris). The hydrodynamic diameters (d_h) and apparent zeta potentials (ζ^{app}) of the AuNPs under these solution conditions are provided in Table 3. At 0.1 M NaCl both types of AuNPs agglomerated to a considerable extent; however, nanoparticle agglomeration state remained stable over the course of QCM-D experiments.

Attachment of cationic MPNH$_2$–AuNPs was observed for all supported lipid bilayers at both NaCl concentrations (Fig. 6) and was irreversible with respect to dilution (rinsing with AuNP-free buffer for 20 min). Attachment of the MPNH$_2$–AuNPs to the bilayers studied can be attributed to Coulombic attraction of the positively charged nanoparticles to negative surface potential of the bilayers. The ζ^{app} for the MPNH$_2$-AuNPs was positive at both NaCl concentrations (26 ± 1 mV). Prior streaming current studies demonstrated that ζ values at pH 7.45 for pure DOPC bilayers on planar silica substrates were negative: −39 ± 1 mV for 0.001 M KCl and −17.5 ± 0.7 mV for 0.01 M KCl.[71] Streaming current measurements

This journal is © The Royal Society of Chemistry 2016

Environ. Sci.: Nano, 2016, **3**, 45–55 | 51

Table 3 Hydrodynamic diameter (d_h) and apparent zeta potential (ζ^{app}) values of AuNPs used in this study. Data are presented for both 0.001 and 0.1 M NaCl, pH 7.4 (0.01 M Tris) buffer conditions. Considerable aggregation occurred for both AuNPs at high ionic strength; however, the aggregate size was consistent throughout the period of particle flow in QCM-D experiments

AuNPs	d_h (nm)		ζ^{app} (mV)	
	0.001 M NaCl	0.1 M NaCl	0.001 M NaCl	0.1 M NaCl
MPA–AuNP	22 ± 10	160 ± 26	−21 ± 5	−28 ± 1
MPNH$_2$–AuNP	6 ± 3	440 ± 120	26 ± 1	26 ± 1

of pure DOPC bilayers at 0.1 M KCl were not made in the referenced study, but ζ values at this salt concentration are expected to be somewhat less negative. (We note that at pH ~7.4 ζ is not expected to differ appreciably between solutions composed of KCl and NaCl.)[72] The ζ of the DOPC/SM/Chol vesicles were similar to those composed of solely DOPC (identical at 0.1 M NaCl; Table 1). This comparison leads to the expectation that the DOPC/SM/Chol and pure DOPC supported lipid bilayers possessed similarly negative ζ values. Incorporation of the anionic glycosphingolipid G$_{M1}$ at 1 mol% resulted in small unilamellar vesicles with slightly more negative ζ values than in its absence (Table 1). In the present study, solutions were buffered with Tris. At the pH of the solutions used, TrisH$^+$ cations were present at 0.008 M, and these cations are present at the SiO$_2$–water interface,[31] likely leading to slightly less negative ζ values than indicated from the streaming current data. Second harmonic

Fig. 6 Attachment of MPNH$_2$–AuNP to supported lipid bilayers of the indicated compositions. The molar ratio of DOPC to SM to Chol was 60 : 20 : 20. Ganglioside GM1 was incorporated into vesicles at 1 mol%. Solutions were buffered to pH 7.4 with 0.01 M Tris and contained the indicated amount of NaCl. The Δf values are for the 5th harmonic and represent the change in frequency from the supported lipid bilayer value after flowing 10 nM MPNH$_2$–AuNPs for 20 min and rinsing with buffer for 20 min. Nanoparticle detachment was not observed upon rinsing with buffer. Letters indicate significant differences in attachment ($p < 0.05$) within each NaCl treatment. Bars represent mean values; error bars represent one standard deviation ($n = 3$).

generation studies of phosphatidylcholine bilayers in the presence of Tris have shown that the surface potential remains negative at the solution conditions investigated here.[31] For all bilayers investigated, the extent of attachment was much larger at 0.001 M than at 0.1 M NaCl. For example, $\Delta f_5/5 = -242 \pm 23$ Hz at 0.001 M NaCl and -10.0 ± 1.0 Hz at 0.1 M NaCl for attachment to supported lipid bilayers composed of 60/20/20 mol% DOPC/SM/Chol. The larger amount of MPNH$_2$-AuNP attachment at 0.001 M relative to 0.1 M NaCl is due to the more negative ζ of the bilayer (*vide supra*) and the lower degree of nanoparticle aggregation (Table 3) at the lower ionic strength. At 0.001 M NaCl, 20 min exposure of the bilayers to MPNH$_2$–AuNPs resulted in frequency changes corresponding to numbers of attached particles exceeding the jamming limit expected from random sequential adsorption of uniform, non-interacting spheres.[73]

At 0.001 M NaCl, MPNH$_2$–AuNP attachment to all supported lipid bilayers investigated, as well as initial rates of nanoparticle attachment (Fig. S3†), were statistically indistinguishable ($p > 0.1$). In contrast, at 0.1 M NaCl attachment to bilayers containing L$_o$ domains was higher than that to pure DOPC bilayers ($p < 0.01$). For lipid bilayers containing L$_o$ domains, $\Delta f_5/5 = -10.0 \pm 1.0$ Hz and -8.2 ± 2.6 Hz in the absence and presence of 1 mol% G$_{M1}$. For pure DOPC bilayers, $\Delta f_5/5 = -1.1 \pm 0.5$ Hz. The extent of attachment to L$_o$ domain-containing supported lipid bilayers was not affected by the presence of G$_{M1}$ ($p > 0.1$).

The higher attachment of MPNH$_2$-AuNPs to bilayers containing L$_o$ domains relative to those lacking these structures may be attributable to differences in bilayer morphology. At 0.1 M NaCl, the DOPC and DOPC/SM/Chol vesicles possessed identical ζ values (Table 1), and the supported lipid bilayers are expected to exhibit similar ζ values as well. This argues against differences in bilayer ζ being responsible for the higher attachment to the DOPC/SM/Chol relative to DOPC bilayers. We hypothesize that differences in supported lipid bilayer morphology are responsible for the higher attachment to the L$_o$ domain-containing bilayers. The L$_o$ and L$_d$ regions differ in height by approximately 1 nm (*vide supra*). This height difference occurs over a lateral distance of approximately 10–15 nm, and the altered water structure at this boundary may result in increased nanoparticle attachment.[74] Alternatively, this boundary region may result in the exposure of sphingomyelin phosphate groups at the edges of L$_o$ domains, providing local sites for increased electrostatic attraction with the cationic MPNH$_2$–AuNPs. The G$_{M1}$ molecule carries a negative charge; however, the ζ data for the vesicles show that incorporation of this glycosphingolipid into vesicles at 1 mol% produced a slight, but significant, reduction in ζ ($p < 0.01$; Table 1). In the QCM-D experiments, MPNH$_2$–AuNP attachment to L$_o$ domain-containing bilayers was insensitive to inclusion of 1 mol% G$_{M1}$ ($p > 0.1$). This result provides further evidence that the presence of domains or their boundaries, not the overall surface potential of the bilayer, is responsible for the increase in attachment for L$_o$ domain-containing supported lipid bilayers.
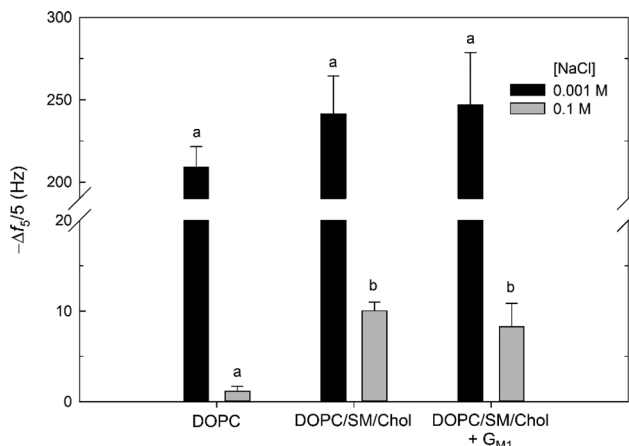
No attachment of anionic MPA-AuNPs was detectable at either NaCl concentration for the bilayers studied. This result can be rationalized by considering the negative ζ^{app} of the nanoparticles (-21 ± 5 mV and -28 ± 1 mV for 0.001 and 0.1 M NaCl) and those expected for the bilayers (*vide supra*). We conclude that Coulombic repulsion prevented detectable attachment. The ζ for the MPA–AuNPs were large and negative under the solution conditions employed. We cannot exclude the attachment of MPA–AuNPs to the bilayers employed at amounts below the limit of QCM-D detection as we demonstrated in prior work for pure DOPC bilayers.[31]

Conclusions

Cellular membranes across all domains of life appear to exhibit lateral organization,[12,26–28] and lipid rafts have been implicated as important membrane organizing structures.[12,16,75] Knowledge of the diverse functions of lipid rafts in cellular membranes is expanding as the development and refinement of instrumentation allows these structures to be studied at minute length and time scales.[18] At present strong evidence exists for the participation of lipid rafts in T-cell signaling,[76] post-Golgi traffic to the cell surface,[23] and glycosphingolipid-mediated endocytosis.[24] Giant unilamellar vesicles formed from plasma membranes exhibit phase-segregated domains similar to those in model membranes.[77–79] These similarities and the participation of lipid rafts in a large number of cellular processes justify the development of supported lipid bilayers to simulate these domains in cellular membranes, thereby enabling their study with a wider array of instrumentation. In this study we have demonstrated the ability to form L_o domain-containing supported lipid bilayers on silica substrates, permitting investigation of these domains by a variety of surface-sensitive techniques such as QCM-D, AFM, ellipsometry, electrochemical impedance spectroscopy, secondary ion mass spectrometry, and non-linear optical methods. The variety of techniques available to probe surfaces makes possible the investigation of dynamics occurring at the interface between phase-segregated regions, including protein incorporation,[80,81] association of viruses,[82,83] and interaction with nanoparticles (as demonstrated in this work). Furthermore, development of supported lipid bilayers that contain other domain-forming lipids (*e.g.*, ceramides)[84] and proteins that segregate to domains (*e.g.*, glycophosphatidylinositol-anchored proteins)[12] will enable investigation of the role such components play in the dynamic processes occurring at the lipid raft-solution interface.

Observations of differential nanoparticle attachment to L_o domain-containing bilayers, relative to those containing one phospholipid in a continuous phase, both provide a foundation and highlight the need for further investigations of nanoparticle interaction with phase-segregated domains. Future investigation into the influence of nanoparticle size, shape, surface chemistry, and degree of aggregation on interaction with phase-segregated domains, as well as with domain-associating proteins, is warranted. Such studies would improve our understanding of the extent to which phase-segregated domains and their components govern nanoparticle interactions with cellular membranes.

Acknowledgements

Notes and references

1 M. A. Maurer-Jones, I. L. Gunsolus, C. J. Murphy and C. L. Haynes, *Anal. Chem.*, 2013, **85**, 3036–3049.

2 A. E. Nel, L. Mädler, D. Velegol, T. Xia, E. M. V. Hoek, P. Somasundaran, F. Klaessig, V. Castranova and M. Thompson, *Nat. Mater.*, 2009, **8**, 543–557.

3 C. C. Berry and A. S. Curtis, *J. Phys. D: Appl. Phys.*, 2003, **36**, 198–206.

4 A. Verma and F. Stellacci, *Small*, 2010, **6**, 12–21.

5 P. R. Leroueil, S. Hong, A. Mecke, J. R. Baker, B. G. Orr and M. M. Banaszak Holl, *Acc. Chem. Res.*, 2007, **40**, 335–342.

6 J. Chen, J. A. Hessler, K. Putchakayala, B. K. Panama, D. P. Khan, S. Hong, D. G. Mullen, S. C. DiMaggio, A. Som, G. N. Tew, A. N. Lopatin, J. R. Baker, M. M. Banaszak Holl and B. G. Orr, *J. Phys. Chem. B*, 2009, **113**, 11179–11185.

7 T. Xia, M. Kovochich, J. Brant, M. Hotze, J. Sempf, T. Oberley, C. Sioutas, J. I. Yeh, M. R. Wiesner and A. E. Nel, *Nano Lett.*, 2006, **6**, 1794–1807.

8 Z. Wang, N. Li, J. Zhao, J. C. White, P. Qu and B. Xing, *Chem. Res. Toxicol.*, 2012, **25**, 1512–1521.

9 M. Luckey, *Membrane Structural Biology with Biochemical and Biophysical Foundations*, 2nd edn, Cambridge University Press, Cambridge, UK, 2014.

10 O. Quehenberger, A. M. Armando, A. H. Brown, S. B. Milne, D. S. Myers, A. H. Merrill, S. Bandyopadhyay, K. N. Jones, S. Kelly, R. L. Shaner, C. M. Sullards, E. Wang, R. C. Murphy, R. M. Barkley, T. J. Leiker, C. R. H. Raetz, Z. Guan, G. M. Laird, D. A. Six, D. W. Russell, J. G. McDonald, S. Subramaniam, E. Fahy and E. A. Dennis, *J. Lipid Res.*, 2010, **51**, 3299–3305.

11 J. A. F. Op den Kamp, *Annu. Rev. Biochem.*, 1979, **48**, 47–71.

12 D. A. Brown and E. London, *Annu. Rev. Cell Dev. Biol.*, 1998, **14**, 111–136.

13 D. L. Nelson and M. M. Cox, *Lehninger Principles of Biochemistry*, 3rd edn, Worth Publishers, New York, 2000.

14 G. Van Meer, D. R. Voelker and G. W. Feigenson, *Nat. Rev. Mol. Cell Biol.*, 2008, **9**, 112–124.

15 R. F. M. De Almeida, A. Fedorov and M. Prieto, *Biophys. J.*, 2003, **85**, 2406–2416.

16 K. Simons and E. Ikonen, *Nature*, 1997, **387**, 569–572.

17 J. F. Hancock, *Nat. Rev. Mol. Cell Biol.*, 2006, **7**, 456–462.

This journal is © The Royal Society of Chemistry 2016

Environ. Sci.: Nano, 2016, **3**, 45–55 | 53

18 K. Simons and M. J. Gerl, *Nat. Rev. Mol. Cell Biol.*, 2010, **11**, 688–699.

19 S. L. Veatch, P. Cicuta, P. Sengupta, A. Honerkamp-Smith, D. Holowka and B. Baird, *ACS Chem. Biol.*, 2008, **3**, 287–293.

20 P.-F. Lenne, L. Wawrezinieck, F. Conchonaud, O. Wurtz, A. Boned, X.-J. Guo, H. Rigneault, H.-T. He and D. Marguet, *EMBO J.*, 2006, **25**, 3245–3256.

21 L. J. Pike, *J. Lipid Res.*, 2006, **47**, 1597–1598.

22 D. M. Owen, A. Magenau, D. Williamson and K. Gaus, *BioEssays*, 2012, **34**, 739–747.

23 T. Weimbs, S. Low, S. Chapin and K. Mostov, *Trends Cell Biol.*, 1997, **8924**, 393–399.

24 S. Mukherjee, T. T. Soe and F. R. Maxfield, *J. Cell Biol.*, 1999, **144**, 1271–1284.

25 D. A. Brown and E. London, *J. Biol. Chem.*, 2000, **275**, 17221–17224.

26 J. L. Cacas, F. Furt, M. Le Guédard, J. M. Schmitter, C. Buré, P. Gerbeau-Pissot, P. Moreau, J. J. Bessoule, F. Simon-Plas and S. Mongrand, *Prog. Lipid Res.*, 2012, **51**, 272–299.

27 X. Xu, R. Bittman, G. Duportail, D. Heissler, C. Vilcheze and E. London, *J. Biol. Chem.*, 2001, **276**, 33540–33546.

28 M. Bramkamp and D. Lopez, *Microbiol. Mol. Biol. Rev.*, 2015, **79**, 81–100.

29 K. Chen and G. Bothun, *Environ. Sci. Technol.*, 2014, **48**, 873–880.

30 P. Yi and K. L. Chen, *Environ. Sci. Technol.*, 2013, **47**, 5711–5719.

31 J. M. Troiano, L. L. Olenick, T. R. Kuech, E. S. Melby, D. Hu, S. E. Lohse, A. C. Mensch, M. Dogangun, A. M. Vartanian, M. D. Torelli, E. Ehimiaghe, S. R. Walter, L. Fu, C. R. Anderton, Z. Zhu, H. Wang, G. Orr, C. J. Murphy, R. J. Hamers, J. A. Pedersen and F. M. Geiger, *J. Phys. Chem. C*, 2015, **119**, 534–546.

32 N.-J. Cho, C. W. Frank, B. Kasemo and F. Höök, *Nat. Protoc.*, 2010, **5**, 1096–1106.

33 R. P. Richter, R. Berat and A. R. Brisson, *Langmuir*, 2006, **22**, 3497–3505.

34 K. El Kirat, S. Morandat and Y. F. Dufrêne, *Biochim. Biophys. Acta*, 2010, **1798**, 750–765.

35 A. Mecke, I. J. Majoros, A. K. Patri, J. R. Baker, M. M. Banaszak Holl and B. G. Orr, *Langmuir*, 2005, **21**, 10348–10354.

36 A. Mecke, D. K. Lee, A. Ramamoorthy, B. G. Orr and M. M. Banaszak Holl, *Langmuir*, 2005, **21**, 8588–8590.

37 P. R. Leroueil, S. A. Berry, K. Duthie, G. Han, V. M. Rotello, D. Q. McNerny, J. R. Baker, B. G. Orr and M. M. Banaszak Holl, *Nano Lett.*, 2008, **8**, 420–424.

38 S. Hong, P. R. Leroueil, E. K. Janus, J. L. Peters, M. M. Kober, M. T. Islam, B. G. Orr, J. R. Baker and M. M. Banaszak Holl, *Bioconjugate Chem.*, 2006, **17**, 728–734.

39 R. C. Van Lehn, M. Ricci, P. H. J. Silva, P. Andreozzi, J. Reguera, K. Voïtchovsky, F. Stellacci and A. Alexander-Katz, *Nat. Commun.*, 2014, **5**, 4482.

40 C. Yuan, J. Furlong, P. Burgos and L. J. Johnston, *Biophys. J.*, 2002, **82**, 2526–2535.

41 C. Dietrich, L. A. Bagatolli, Z. N. Volovyk, N. L. Thompson, M. Levi, K. Jacobson and E. Gratton, *Biophys. J.*, 2001, **80**, 1417–1428.

42 M. Sundh, S. Svedhem and D. S. Sutherland, *Phys. Chem. Chem. Phys.*, 2010, **12**, 453–460.

43 J. P. Slotte, *Prog. Lipid Res.*, 2013, **52**, 424–437.

44 P. J. Quinn, *Langmuir*, 2013, **29**, 9447–9456.

45 R. Richter, A. Mukhopadhyay and A. Brisson, *Biophys. J.*, 2003, **85**, 3035–3047.

46 M. M. Lapinski, A. Castro-Forero, A. J. Greiner, R. Y. Ofoli and G. J. Blanchard, *Langmuir*, 2007, **23**, 11677–11683.

47 S. F. Sweeney, G. H. Woehrle and J. E. Hutchison, *J. Am. Chem. Soc.*, 2006, **128**, 3190–3197.

48 L. Zhu, C. Zhang, C. Guo, X. Wang, P. Sun, D. Zhou, W. Chen and G. Xue, *J. Phys. Chem. C*, 2013, **117**, 11399–11404.

49 W. Haiss, N. T. K. Thanh, J. Aveyard and D. G. Fernig, *Anal. Chem.*, 2007, **79**, 4215–4221.

50 M. Rodahl, F. Höök, A. Krozer, P. Brzezinski and B. Kasemo, *Rev. Sci. Instrum.*, 1995, **66**, 3924–3930.

51 C. A. Keller and B. Kasemo, *Biophys. J.*, 1998, **75**, 1397–1402.

52 K. H. Jacobson, T. R. Kuech and J. A. Pedersen, *Environ. Sci. Technol.*, 2013, **47**, 6925–6934.

53 W. S. Cleveland and S. J. Devlin, *J. Am. Stat. Assoc.*, 1988, **83**, 596–610.

54 S. Ladha, A. R. Mackie, L. J. Harvey, D. C. Clark, E. J. Lea, M. Brullemans and H. Duclohier, *Biophys. J.*, 1996, **71**, 1364–1373.

55 J. Yguerabide, J. A. Schmidt and E. E. Yguerabide, *Biophys. J.*, 1982, **40**, 69–75.

56 D. Nečas and P. Klapetek, *Cent. Eur. J. Phys.*, 2011, **10**, 181–188.

57 S. Chiantia, N. Kahya, J. Ries and P. Schwille, *Biophys. J.*, 2006, **90**, 4500–4508.

58 M. G. Gustafsson, *J. Microsc.*, 2000, **198**, 82–87.

59 B. Bailey, D. L. Farkas, D. L. Taylor and F. Lanni, *Nature*, 1993, **366**, 44–48.

60 A. R. Burns, D. J. Frankel and T. Buranda, *Biophys. J.*, 2005, **89**, 1081–1093.

61 J. Holmgren, I. Lönnroth, J.-E. Månsson and L. Svennerholm, *Proc. Natl. Acad. Sci. U. S. A.*, 1975, **72**, 2520–2524.

62 W. I. Lencer, *Am. J. Physiol.*, 2001, **280**, G781–G786.

63 N.-J. Cho, L. Hwang, J. Solandt and C. Frank, *Materials*, 2013, **6**, 3294–3308.

64 C. Hamai, P. S. Cremer and S. M. Musser, *Biophys. J.*, 2007, **92**, 1988–1999.

65 C. Hamai, T. Yang, S. Kataoka, P. S. Cremer and S. M. Musser, *Biophys. J.*, 2006, **90**, 1241–1248.

66 N. Kahya, D. Scherfeld, K. Bacia, B. Poolman and P. Schwille, *J. Biol. Chem.*, 2003, **278**, 28109–28115.

67 A. V. Samsonov, I. Mihalyov and F. S. Cohen, *Biophys. J.*, 2001, **81**, 1486–1500.

68 Y. Lange, J. Dolde and T. L. Steck, *J. Biol. Chem.*, 1981, **256**, 5321–5323.

69 E. Reimhult, F. Höök and B. Kasemo, *J. Chem. Phys.*, 2002, **117**, 7401–7404.

70 C. A. Keller, K. Glasmästar, V. P. Zhdanov and B. Kasemo, *Phys. Rev. Lett.*, 2000, **84**, 5443–5446.

54 | *Environ. Sci.: Nano*, 2016, **3**, 45–55

This journal is © The Royal Society of Chemistry 2016

71 R. Zimmermann, D. Küttner, L. Renner, M. Kaufmann, J. Zitzmann, M. Müller and C. Werner, *Biointerphases*, 2009, **4**, 1–6.

72 R. Zimmermann, D. Küttner, L. Renner, M. Kaufmann and C. Werner, *J. Phys. Chem. A*, 2012, **116**, 6519–6525.

73 Z. Adamczyk, *Particles at Interfaces: Interactions, Deposition, Structure*, Academic Press, San Diego, CA, 2006.

74 K. H. Sheikh and S. P. Jarvis, *J. Am. Chem. Soc.*, 2011, **133**, 18296–18303.

75 R. G. W. Anderson and K. Jacobson, *Science*, 2002, **296**, 1821–1825.

76 M. C. Seminario and S. C. Bunnell, *Immunol. Rev.*, 2008, **221**, 90–106.

77 T. Baumgart, A. T. Hammond, P. Sengupta, S. T. Hess, D. A. Holowka, B. A. Baird and W. W. Webb, *Proc. Natl. Acad. Sci. U. S. A.*, 2007, **104**, 3165–3170.

78 I. Leventhal, F. J. Byfield, P. Chowdhury, F. Gai, T. Baumgart and P. A. Janmey, *Biochem. J.*, 2009, **424**, 163–167.

79 D. Lingwood, J. Ries, P. Schwille and K. Simons, *Proc. Natl. Acad. Sci. U. S. A.*, 2008, **105**, 10005–10010.

80 P. Sharma, R. Varma, R. C. Sarasij, Ira, K. Gousset, G. Krishnamoorthy, M. Rao and S. Mayor, *Cell*, 2004, **116**, 577–589.

81 N. Vyas, D. Goswami, A. Manonmani, P. Sharma, H. A. Ranganath, K. VijayRaghavan, L. S. Shashidhara, R. Sowdhamini and S. Mayor, *Cell*, 2008, **133**, 1214–1227.

82 A. A. Waheed and E. O. Freed, *Virus Res.*, 2009, **143**, 162–176.

83 P. Scheiffele, A. Rietveld, K. Simons and T. Wilk, *J. Biol. Chem.*, 1999, **274**, 2038–2044.

84 B. M. Castro, M. Prieto and L. C. Silva, *Prog. Lipid Res.*, 2014, **54**, 53–67.